Earthquakes and Structures, Vol. 3, No. 6 (2012) 821-838
DOI: http://dx.doi.org/10.12989/eas.2012.3.6.821

New three-layer-type hysteretic damper system and its damping capacity

Hyeong Gook Kim[1], Shinta Yoshitomi[2], Masaaki Tsuji[2] and Izuru Takewaki*[2]

[1]Department of Urban and Environmental Engineering, Kyoto University, Japan
[2]Department of Architecture and Architectural Engineering, Graduate School of Engineering, Kyoto University, Kyotodaigaku-Katsura, Nishikyo-ku, Kyoto 615-8540, Japan

(Received November 14, 2011, Revised May 17, 2012, Accepted May 18, 2012)

Abstract. This paper proposes a new three-layer pillar-type hysteretic damper system for residential houses. The proposed vibration control system has braces, upper and lower frames and a damper unit including hysteretic dampers. The proposed vibration control system supplements the weaknesses of the previously proposed post-tensioning vibration control system in the damping efficiency and cumbersomeness of introducing a post-tension. The structural variables employed in the damper design are the stiffness ratio κ, the ductility ratio μ_a, and the ratio β of the damper's shear force to the maximum resistance. The hysteretic dampers are designed so that they exhibit the targeted damping capacity at a specified response amplitude. Element tests of hysteretic dampers are carried out to examine the mechanical property and to compare its restoring-force characteristic with that of the analytical model. Analytical studies using an equivalent linearization method and time-history response analysis are performed to investigate the damping performance of the proposed vibration control system. Free vibration tests using a full-scale model are conducted in order to verify the damping capacity and reliability of the proposed vibration control system. In this paper, the damping capacity of the proposed system is estimated by the logarithmic decrement method for the response amplitudes. The accuracy of the analytical models is evaluated through the comparison of the test results with those of analytical studies.

Keywords: pillar-type hysteretic damper system; stiffness ratio; ductility ratio; damper's shear force; free vibration test; geometrical nonlinearity; logarithmic decrement method

1. Introduction

Passive control devices (viscous, visco-elastic, hysteretic, friction, tuned-mass etc) are often incorporated into building structures in order to resist the energy input from earthquake ground motions (for example, see Aiken *et al.* 1993, Housner *et al.* 1997, Hanson and Soong 2001, Christopoulos and Filiatrault 2006, Takewaki 2009). The main roles of passive control devices are to dissipate the input energy from earthquakes, keeping the main structural members undamaged or with minor damage and maintaining the serviceability of structures. Hysteretic dampers are one of the well-used and accepted passive control devices applied to building structures (for example, see Moreschi and Singh 2003, Kim and Seo 2004, Li and Li 2007, Chan and Albermani 2008, Oh *et al.*

*Corresponding author, Professor, E-mail: takewaki@archi.kyoto-u.ac.jp

2008, Apostolakis and Dargush 2010, Benavent-Climent 2011). The hysteretic dampers can dissipate the input energy by its yielding (Skinner *et al*. 1975, Yamaguchi and El-Abd 2003, Takewaki 2009).

Although damping systems with hysteretic dampers have been widely used in multi-storey buildings and residential houses, some problems remain unresolved which are due to cost and difficulties in control and tuning. The purpose of this paper is to propose a new vibration control system which has high damping capacities and reliable advantages for wind and earthquake disturbances with low cost and ease in installation. The control system is a three-layer pillar-type hysteretic damper system and supplements the weaknesses of the previously proposed post-tensioning vibration control system (Tsuji *et al*. 2010) resulting from its low damping efficiency and cumbersomeness of introducing post-tension.

The structural variables used in its damper design are the stiffness ratio κ, the ductility ratio μ_a, and the ratio β of the damper's shear force to the maximum resistance (Nakashima *et al*. 1996, Inoue and Kuwahara 1998). Hysteretic dampers are designed so that they exhibit the targeted damping capacity at a specified response. The standard and extended cases of hysteretic dampers are introduced to compare its damping capacity with that of a similar system including high-hardness rubber dampers (Tani *et al*. 2009). Element tests of hysteretic dampers are carried out to examine its mechanical property and to compare its restoring-force characteristic with that of the analytical model. Analytical studies using an equivalent linearization method and time-history response analysis are performed to investigate the damping performance of the proposed vibration control system. Free vibration tests with a full-scale model are conducted in order to verify the validity and damping capacity of the proposed damper system. In this paper, the damping capacity of the proposed system is estimated by the logarithmic decrement method for the response amplitudes. The accuracy of the analytical models is evaluated through the comparison of the test results with those of analytical studies (Kim *et al*. 2011).

2. A new three-layer pillar-type hysteretic damper system

2.1 Outline of the previously proposed post-tensioning damper system

The post-tensioning damper system (Tsuji *et al*. 2010) consists of four braces and a damper unit as shown in Fig. 1(a). Turn-buckles installed in the braces are used to introduce the post-tension in this damper system for helping the functioning of the damper system even in the small vibration range. The post-tensioning vibration control system has an advantage of low cost, high safety and high-level habitability under traffic and small wind vibrations. However, the damping performance of their system is affected by the level of introduced post tensioning forces and the rotation of a damper unit decreases the damping efficiency. Moreover the post-tensioning damper system has a limitation on installation because the optimal installation angle of braces exists, which maximizes the damping efficiency of the damper system. To supplement such weakness, a new three-layer pillar-type hysteretic damper system is proposed.

2.2 Outline of a new three-layer pillar-type hysteretic damper system

A three-layer pillar-type hysteretic damper system, as shown in Fig. 1(b), is proposed, which

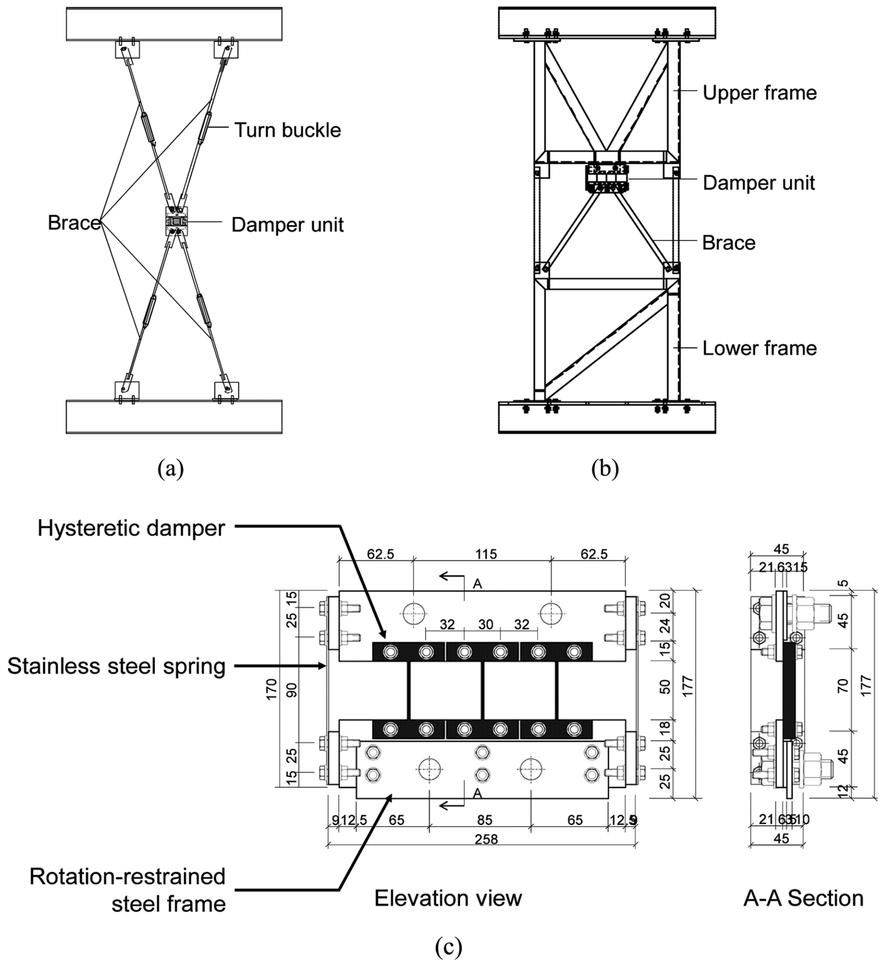

Fig. 1 Comparison of three-layer pillar-type damper system with post-tensioning damper system: (a) post-tensioning damper system, (b) three-layer pillar-type damper system and (c) damper unit (unit: mm)

consists of braces, a damper unit, upper and lower frames. The damper unit is composed of two steel springs, rotation-restrained steel frames and I-type hysteretic dampers as a device for dissipating the input energy from dynamic loadings. The proposed vibration control system here supplements the weaknesses (rotation of the unit) of the previously proposed post-tensioning vibration control system by fixing the damper unit beneath the upper frame as shown in Fig. 1(b).

The proposed three-layer pillar-type system taking the system format of existing wall-type damper systems has an advantage that the change of story height and length of the hysteretic dampers can be adjusted properly by changing the vertical height of the second layer without the change of the size of the upper and lower frames. The surrounding portions (braces, upper and lower frames) are designed to be stiff compared to hysteretic dampers so as to prevent negative effects on damping efficiency due to their deformation. Fig. 2 presents the application examples and the working mechanism of the proposed damping system. High damping efficiency can be obtained by concentrating the relative displacement (δ_D) between the upper and lower frames (also approximately the story deformation δ_a) on the incorporated hysteretic dampers only. Furthermore

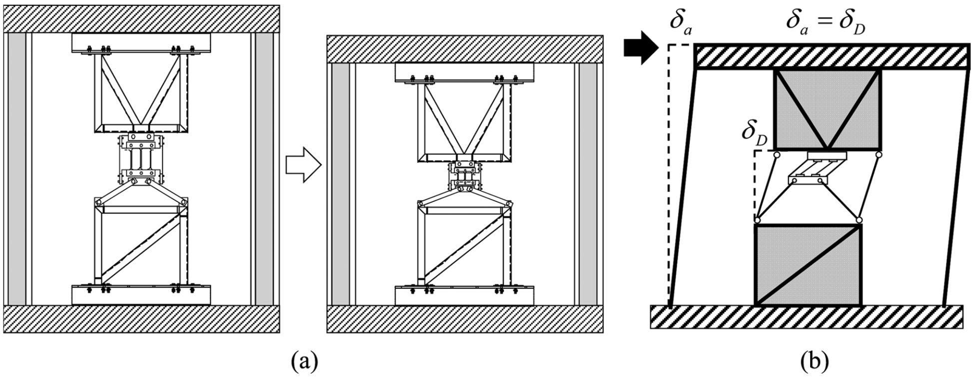

Fig. 2 Application examples and working mechanism of three-layer pillar-type damper system: (a) application of damper system to different story heights and (b) working mechanism

the rotation-restrained steel frames in the damper unit enhances the deformation efficiency of the hysteretic dampers. The removal of post tension helps the reduction of the cross-sectional area of supporting members compared to the post-tensioning vibration control system mentioned above.

2.3 Design of hysteretic damper for various structural variables

The design method of hysteretic dampers is explained. Hysteretic dampers in this paper are designed so that they exhibit the targeted damping capacity at a specified response. The hysteretic behavior of a structural system including a hysteretic damper is simplified as shown in Fig. 3. The entire structural system consists of a moment-resisting steel frame, hereafter called the main frame and a hysteretic damper. In this study, it is assumed that, while the hysteretic damper obeys normal bilinear (elastic-perfectly plastic) hysteretic rules, the main frame does not yield regardless of the increase of shear force. The stiffness ratio κ is defined as

$$\kappa = k_D/k_F \tag{1}$$

where k_F and k_D are the lateral stiffness of the main frame and the hysteretic damper, respectively. The lateral stiffness of the two stainless steel springs in the damper unit is included in the main frame's lateral stiffness k_F. It is intended that the two stainless steel springs do not yield in the deformation amplitude employed in the test. The ductility ratio μ_a is defined as

$$\mu_a=\delta_a/\delta_y \tag{2}$$

where δ_a and δ_y are the elastic deformation of the main frame and the yield point deformation of the hysteretic damper, respectively. The following relations can be obtained by using Fig. 3.

$$\beta = \frac{Q_D}{Q_a} = \frac{Q_D}{Q_F + Q_D} = \frac{k_D\delta_y}{k_F\delta_a + k_D\delta_y} = \frac{\kappa}{\mu_a + \kappa} \tag{3}$$

β in Eq. (3) is the ratio of the damper's shear force to the maximum resistance. Q_a, Q_F and Q_D are the shear forces of the entire structural system, the main frame and the hysteretic damper,

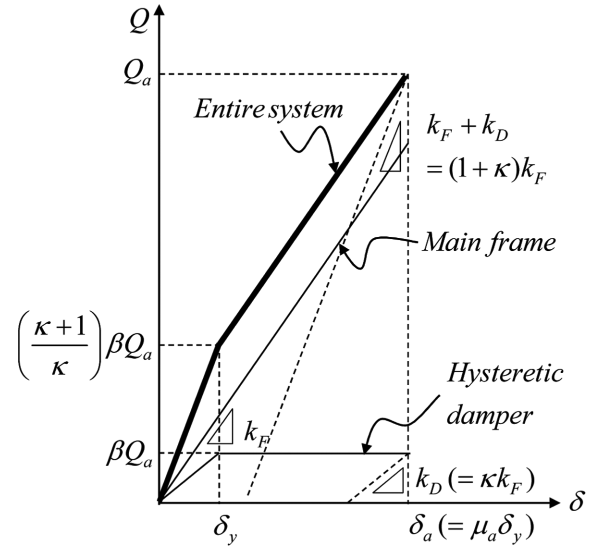

Fig. 3 Restoring-force characteristic of a structure with a hysteretic damper

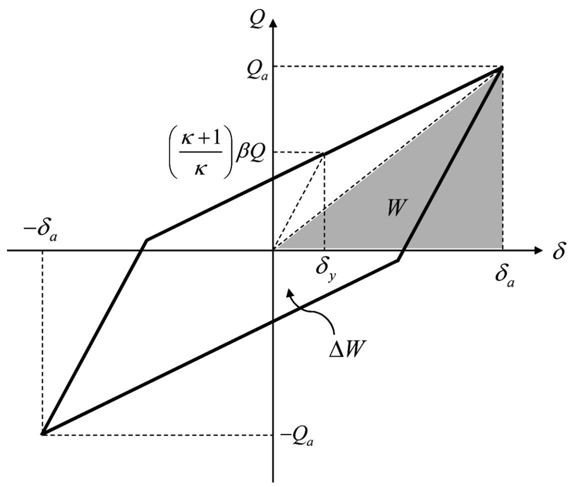

Fig. 4 Hysteretic loop of the entire structural system in the steady state

respectively. These definitions have already been used in many previous researches.

The equivalent damping ratio h_{eq} of the hysteretic loop shown in Fig. 4 is defined as

$$h_{eq} = \frac{\Delta W}{4\pi W} \tag{4}$$

where ΔW and W are the dissipated energy and the maximum potential energy of the entire structural system per cycle, respectively. ΔW and W are expressed in this study as follows

$$\Delta W = 4(\mu_a - 1)\delta_y \beta Q_a \tag{5}$$

$$W = \frac{1}{2}\delta_a Q_a = \frac{1}{2}\mu_a \delta_y Q_a \tag{6}$$

The dissipated energy ΔW of the entire structural system is equivalent to that of an equivalent linear model with a viscous damper. From Eqs. (3)-(6), the equivalent damping ratio h_{eq} is expressed as follows

$$h_{eq} = \frac{2\beta}{\pi}\left[1 - \frac{\beta}{(1-\beta)\kappa}\right] = \frac{2\beta}{\pi}\left[1 - \frac{1}{\mu_a}\right] = \frac{2\kappa}{\pi(\mu_a + \kappa)}\left[1 - \frac{1}{\mu_a}\right] \tag{7}$$

The following equation for the stiffness ratio κ is derived from Eq. (7).

$$\kappa = \frac{\pi\mu_a h_{eq}}{2 - \dfrac{2}{\mu_a} - \pi h_{eq}} = \frac{\pi h_{eq}\mu_a^2}{2(\mu_a - 1) - \pi h_{eq}\mu_a} = \frac{\mu_a}{\dfrac{2(\mu_a - 1)}{\pi h_{eq}\mu_a} - 1} \tag{8}$$

Fig. 5(a) shows the equivalent damping ratio with respect to the ductility ratio for various stiffness ratios κ. It can be understood from Fig. 5(a) that the maximum equivalent damping ratio of hysteretic dampers is proportional to the stiffness ratio. On the other hand, Fig. 5(b) indicates the stiffness ratio κ according to the ductility ratio for various h_{eq}. These results are plotted by using Eq. (8). This result means that there exist the minimum values of the stiffness ratio for each h_{eq}. Using the characteristics of hysteretic dampers on its damping capacity, we design several hysteretic dampers exhibiting a prescribed damping capacity at a specified response.

Before the present study, another research was conducted on the damping performance of the three-layer pillar-type vibration control system with a high-hardness rubber damper (Tani *et al.* 2009). In that research, the equivalent damping ratio h_{eq} was about 4% in the response amplitude range from 2 mm to 4 mm. The cross-sectional area of the high-hardness rubber used in that research was $S = 400\ \mathrm{mm}^2$. We designed a hysteretic damper as the standard case whose equivalent

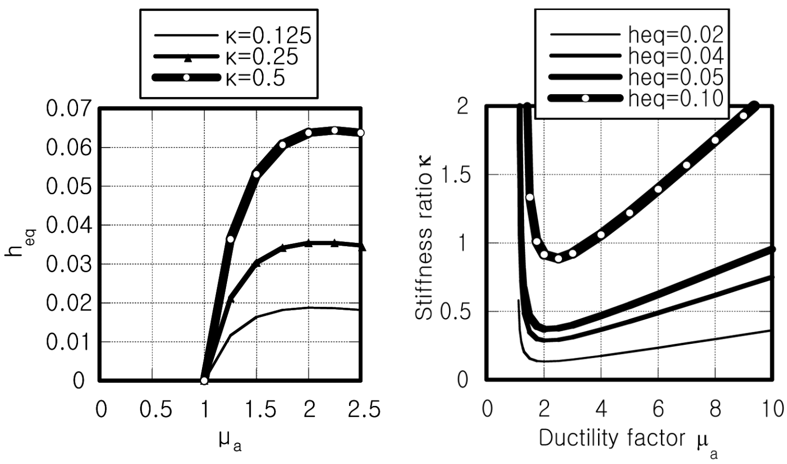

(a) (b)

Fig. 5 Equivalent damping ratio and stiffness ratio with respect to ductility ratio

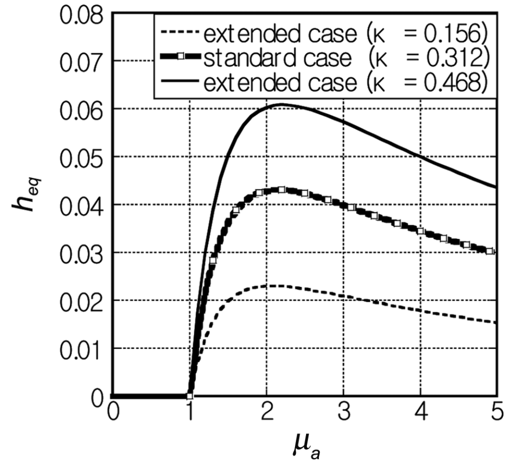

Fig. 6 Equivalent damping ratio with respect to ductility ratio ($\delta_y = 1.0$ mm)

damping ratio is about 4% in the same response amplitude range to compare the equivalent damping ratio of the proposed three-layer pillar-type hysteretic damper system with that of the system including the high-hardness rubber damper. From the given conditions $h_{eq} = 0.04$, $\mu_a = 3.0$ and Eq. (8), the stiffness ratio of the standard case is obtained as $\kappa = 0.312$.

Fig. 6 represents the equivalent damping ratio with respect to the ductility ratio for the standard and extended cases whose stiffness ratios are 0.312, 0.156 and 0.468. The given common yield displacement of the hysteretic dampers is 1.0 mm. This value of yield displacement is given for the convenience of free vibration tests (the maximum allowable displacement in the free vibration test is limited). It can be observed that an optimal ductility factor for maximizing the equivalent damping ratio exists for each stiffness ratio and the parameter set of $h_{eq} = 0.04$, $\mu_a = 3.0$ determined above corresponds with the standard case $\kappa = 0.312$.

3. Mechanical model of proposed system

3.1 Mechanical model of a three-layer pillar-type hysteretic damper system

The proposed three-layer pillar-type hysteretic damper system is represented by a mechanical model as shown in Fig. 7, where k_D, k_S and k_B are the lateral stiffnesses of hysteretic dampers, steel springs and braces, respectively. Furthermore, a building structure with the proposed damper system is modeled into an SDOF model as shown in Fig. 8. The building structure modeled as an SDOF model and hysteretic dampers are assumed to be elastic and normal bilinear, respectively. The stiffness and viscous damping coefficient C^F of the building structure are described as k_F and $C^F = 0$, respectively. Thus, the equivalent stiffness k_{eq} and equivalent damping coefficient C_{eq} of the SDOF model with a hysteretic damper may be described as

(a) $\delta_a \leq \delta_y$

$$k_{eq} = \frac{(k_F + k_D) \times \delta_a}{\delta_a} = k_F + k_D \tag{9}$$

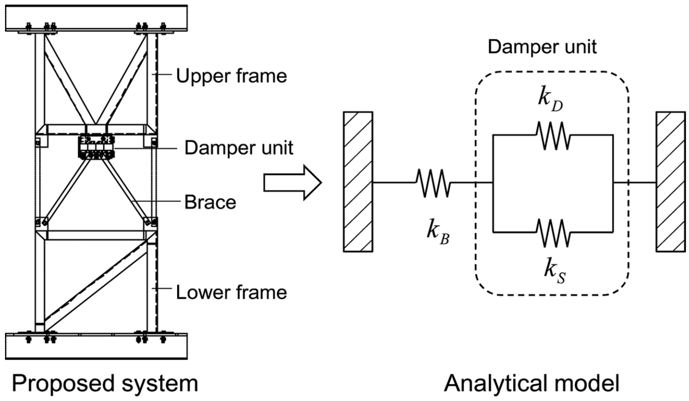

Fig. 7 Proposed three-layer-type hysteretic damper system and its mechanical model

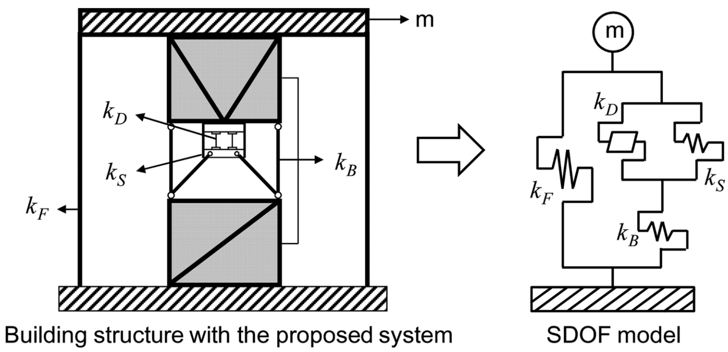

Fig. 8 SDOF model of a building structure with the proposed damper system

$$C_{eq} = C^F + C_{eq}^D = 0 \tag{10}$$

(b) $\delta_a > \delta_y$

$$k_{eq} = \frac{(k_F + k_D) \times \delta_y + k_F(\delta_a - \delta_y)}{\delta_a} = \frac{k_D}{\mu_a} + k_F \tag{11}$$

$$C_{eq} = C^F + C_{eq}^D = 0 + \frac{4k_D}{\pi \omega_{eq} \mu_a}\left(1 - \frac{1}{\mu_a}\right) \tag{12}$$

In Eqs. (9)-(12), δ_a and δ_y are the successively given story drift of a building structure and the yielding point deformation of a hysteretic damper. ω_{eq}, C_{eq}^D are the equivalent natural circular frequency and equivalent viscous damping coefficient of the hysteretic damper, respectively. The lateral stiffnesses of the structural members except hysteretic dampers are given by the values obtained from full-scale model tests with quasi-static and dynamic loadings. The detailed values for the structural members' lateral stiffness and mass will be shown in Section 5. In this paper, the equivalent damping ratios of an SDOF model are evaluated by the logarithmic decrement method for the response amplitudes. Then, the damping performance of the analytical SDOF model is compared with that of the full-scale test.

3.2 Geometrical nonlinearity of hysteretic damper in restoring-force characteristics

Fig. 9 presents the element test of hysteretic dampers and its test result. Before this test, tensile tests of the hysteretic dampers were conducted. The mean yield stress is 292 N/mm^2. The designed hysteretic damper shown in Fig. 9(a) is loaded as shown in Fig. 9(b) with quasi-static speed. Two dampers are used for symmetric configuration. An example of deformed shape is illustrated in Fig. 9(c). A solid line in Fig. 9(d) shows the relation between the shear force and the displacement of the designed hysteretic damper ($\kappa = 0.312$). It can be seen that the relation begins to bend around 1 mm which corresponds to the yield deformation. It is also clear that the effect of plastic behavior of hysteretic dampers is small in the amplitude range larger than 4 mm and the stiffness hardening occurs resulting from a geometrical nonlinearity. The geometrical nonlinearity of the hysteretic damper is caused by the increased axial force. This is the P–Δ effect. A broken line in Fig. 9(d) is the result of an analytical model considering the P–Δ effect and the N-M interaction in the construction of the restoring-force characteristics of the hysteretic damper. It can be observed that the analytical result corresponds to the test result in the range smaller than 4 mm of displacement. The differences between the two results in the deformation range larger than 4 mm are caused by the moment degradation on the N-M interaction after the yield of the hysteretic damper.

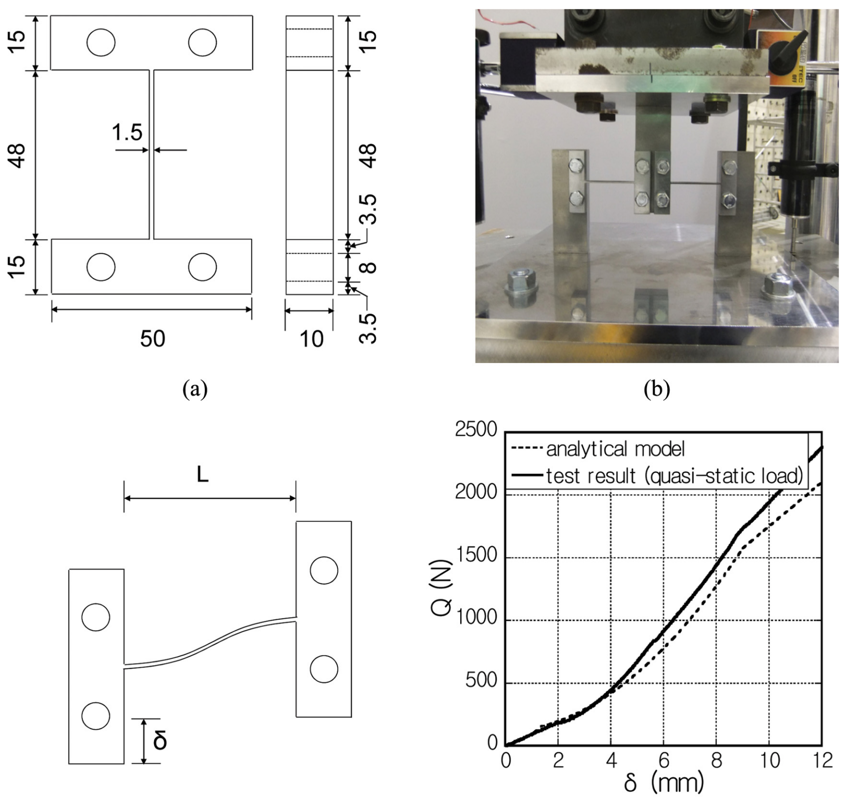

Fig. 9 Element test of hysteretic dampers and its result: (a) overview of hysteretic dampers (unit: mm), (b) element test of hysteretic dampers, (c) deformation in hysteretic damper and (d) comparison of element test result with that of analytical model for Q–δ

This result also leads to the differences of the responses and natural periods between the test and simulations by the SDOF model. However, the geometrical nonlinearity of hysteretic dampers is not considered in the SDOF model and the simulations in order to maintain the convenience in the numerical analysis approach for verifying the damping capacity of the proposed damper system. Only the vibration amplitude smaller than about 4 mm will be considered in the test explained in the following sections.

4. Free vibration test of full-scale model

In order to verify the damping capacity of the proposed damper system, free vibration tests with full-scale models are conducted. The reasons to adopt a free vibration test with full-scale models are as follows; (1) the easiness in evaluating the damping capacity of the proposed vibration control system by the logarithmic decrement method for the response amplitudes, (2) the possibility of assessing the basic performances and the system stability of the surrounding portions and (3) the simplicity of the test system compared to a forced vibration test.

4.1 Purpose of free vibration test

The followings are clarified from the free vibration test; (1) the validity and damping capacity of the proposed damper system, (2) the accuracy of the analytical model and simulation results and (3) the verification of the damping performance in the response range around the yielding point of hysteretic dampers.

4.2 Outline of free vibration test for full-scale model

A full-scale test model (experimental), hereafter called 'a test model', was prepared to verify the validity and damping capacity of the proposed damper system. The natural period of the main frame is the same as that of an existing steel structure whose natural period is $T = 0.37$ s. It should be pointed out that the lateral stiffness and the mass of the test model are different from that of the existing steel structure. It was set up for the easy control of the test model in the free vibration test. The main frame of the test model consists of two steel columns and a steel lump. The main frame is supported by the reaction beams and column frames fixed to the rigid wall by high-strength bolts as shown in Figs. 10(a) and (b). The proposed damper system is installed between two columns of the main frame. The data of displacements and accelerations are measured at the eight points of the test model as shown in Fig. 10(a). The story shear force and the story drift of the main frame are measured at the point $d1$. The horizontal displacement ($d2$-$d3$) between the lower and upper frames is compared to the displacement ($d4$) of the damper unit for evaluating the ratio of the actual deformation of the hysteretic damper to the story drift of the main frame. The shear force in the main frame is evaluated by the inertial force obtained by multiplying the absolute acceleration a_1, a_2 on the mass m of the steel lump ($Q = m \times a_1$, $Q = m \times a_2$).

4.3 Loading program

For the standard and extended cases of hysteretic dampers, the test models were loaded in quasi-

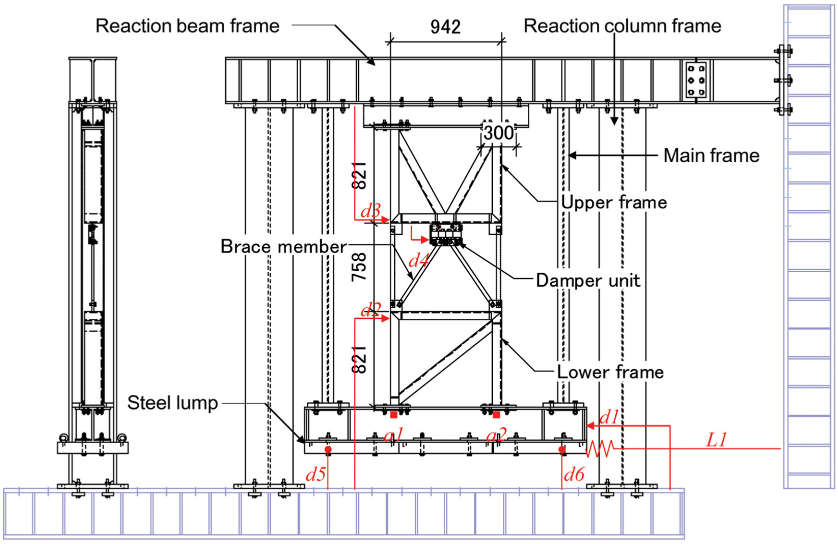

(a)

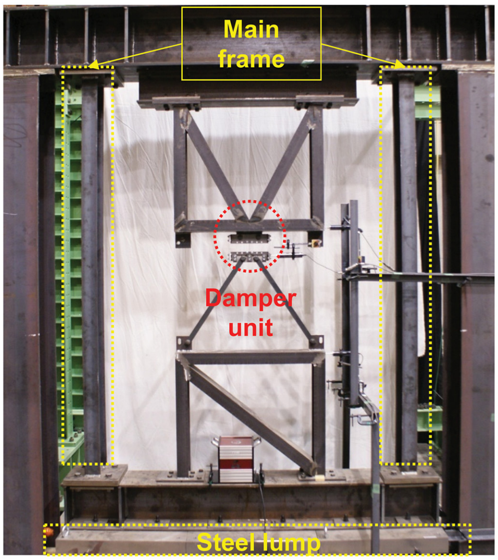

(b)

Fig. 10 (a) Overview of full-scale test and measurement system (unit: mm) and (b) Photo of full-scale test

static speed up to 6 mm of the story-drift by an oil jack at the $L1$ point. The quasi-static loading was carried out to assess the ratio β of the damper's shear force to the maximum resistance. After the quasi-static loading up to 6 mm, we make the test models go into the free vibration state by removing the oil jack. In addition, the free vibration tests for the test model without the damper unit were performed to estimate the structural damping and the lateral stiffness of surrounding portions of the test model. Loading cases for the free vibration test are shown in Table 1.

Table 1 Loading cases for free vibration

Case	Stiffness ratio	Steel springs of damper unit	Loading type
A-1	$\kappa = 0.000$	×	Quasi-static loading → free vibration
A-2	$\kappa = 0.156$	×	
A-3	$\kappa = 0.312$	×	
A-4	$\kappa = 0.468$	×	
B-1	$\kappa = 0.000$	○	
B-2	$\kappa = 0.156$	○	
B-3	$\kappa = 0.312$	○	
B-4	$\kappa = 0.168$	○	

A-1 and B-1 ($\kappa = 0.000$) indicate the test models without hysteretic dampers.
×: no existence and ○ : exist

5. Test results and discussion

5.1 Mechanical property of test model without hysteretic dampers in quasi-static loading

Quasi-static loading tests were carried out for the test model A-1 and B-1. Fig. 11 shows the story shear force of the two test models with respect to the story drift. The difference of lateral stiffness between the two test models may result from the lateral stiffness of the steel springs. It was confirmed that the static lateral stiffnesses are small compared to the design values as shown in Table 3. This is caused by the assumption in the system design that the stiffness of each connection may be rigid.

5.2 Mechanical property of test models without hysteretic dampers in free vibration

The natural period T and the structural damping ratio h_0 of the test model are estimated from the free vibration waves. Table 2 shows the natural period and structural damping ratio for the test

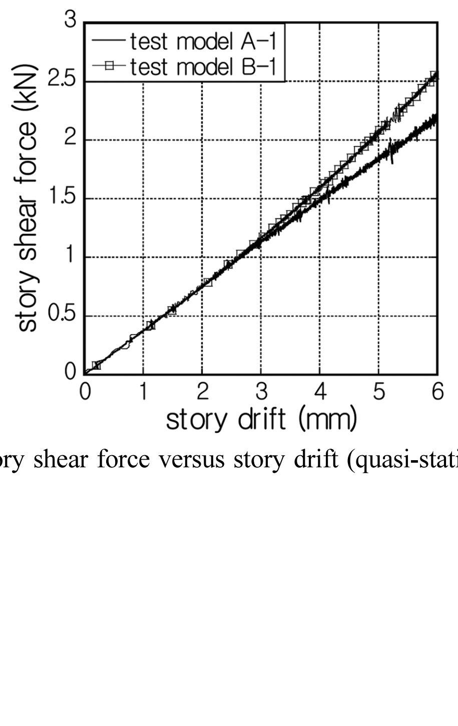

Fig. 11 Story shear force versus story drift (quasi-static loading)

Table 2 Natural period T and structural damping ratio h_0 for different amplitudes

	Test model A-1		Test model B-1	
	T (s)	h_0	T (s)	h_0
4.0 mm~2.0 mm	0.422	0.0023	0.391	0.0024
2.0 mm~1.0 mm	0.422	0.0032	0.406	0.0032
1.0 mm~0.5 mm	0.421	0.0045	0.407	0.0047
0.5 mm~0.2 mm	0.420	0.0061	0.406	0.0059
Average	0.421	0.0040	0.403	0.0040

Table 3 Lateral stiffness dependent on loading types

	Test model A-1 (N/mm)	Test model B-1 (N/mm)	Lateral stiffness (N/mm)	
			Main frame	Steel springs
Design	477	697	477	220
Quasi-static loading	362	424	362	62
Dynamic loading	363	396	363	33

model A-1 and B-1 with respect to different amplitudes. It is understood that the average of the structural damping ratio is $h_0 = 0.0040$. Also, the dynamic lateral stiffnesses of the main frame of the test model and steel springs can be obtained from the average of the natural periods. The lateral stiffnesses of the main frame and the steel spring dependent on load types are shown in Table 3.

5.3 Shear force in hysteretic dampers in quasi-static loading

The shear forces in hysteretic dampers under the quasi-static loading are indicated in Fig. 12. The shear force Q_D in hysteretic dampers is expressed as follow

$$Q_D = Q_a - (K_S + K_F)\delta_a \tag{13}$$

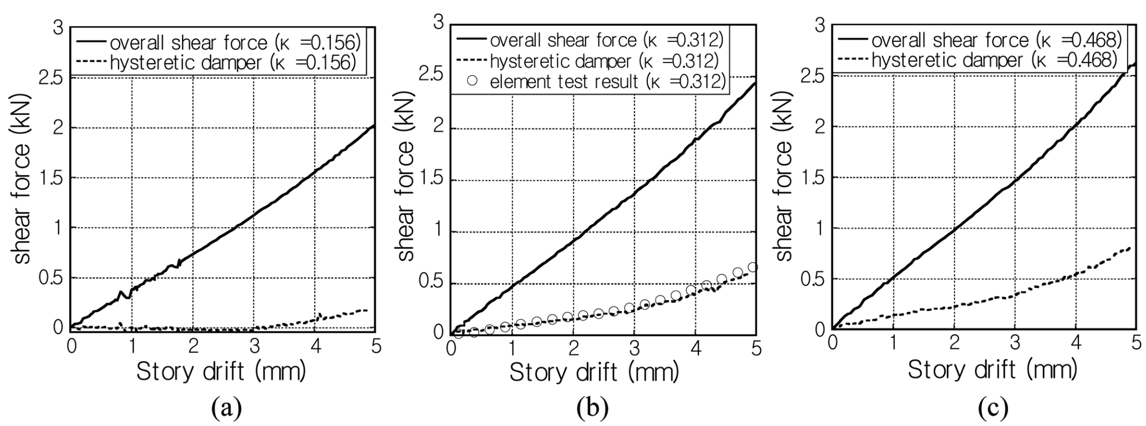

Fig. 12 Overall shear force and damper's shear force versus story drift (Quasi-static loading): (a) $\kappa = 0.156$, (b) $\kappa = 0.312$ and (c) $\kappa = 0.468$

In Eq. (13), Q_a, Q_D, k_S, k_F and δ_a are the test model's shear force, the hysteretic damper's shear force, the steel springs' lateral stiffness, the main frame's lateral stiffness and the story drift of the test model. The broken line in each figure indicates the hysteretic damper's shear force. Here, the geometrical nonlinearity of the hysteretic dampers can be confirmed in all the cases again. The hysteretic damper's shear force for the standard case corresponds with the element test results denoted by open circles in Fig. 12(b). However, it is also understood that the effect of the geometrical nonlinearity on the test model's shear force is small in all the cases. Especially, in the case of $\kappa = 0.156$, the damper's shear force is extremely small in the amplitude range from 0 to 3 mm. It means that the hysteretic damper ($\kappa = 0.156$) could give small effects on the damping capacity and restoring-force characteristics of the entire system.

5.4 Estimation of equivalent damping ratio

Fig. 13 shows the free vibration waves of the test models and simulations. The simulation has been conducted by the general-purpose elastic-plastic analysis program called SNAP (Kozo System 2011). The damping capacity of the test models is estimated by the logarithmic decrement method

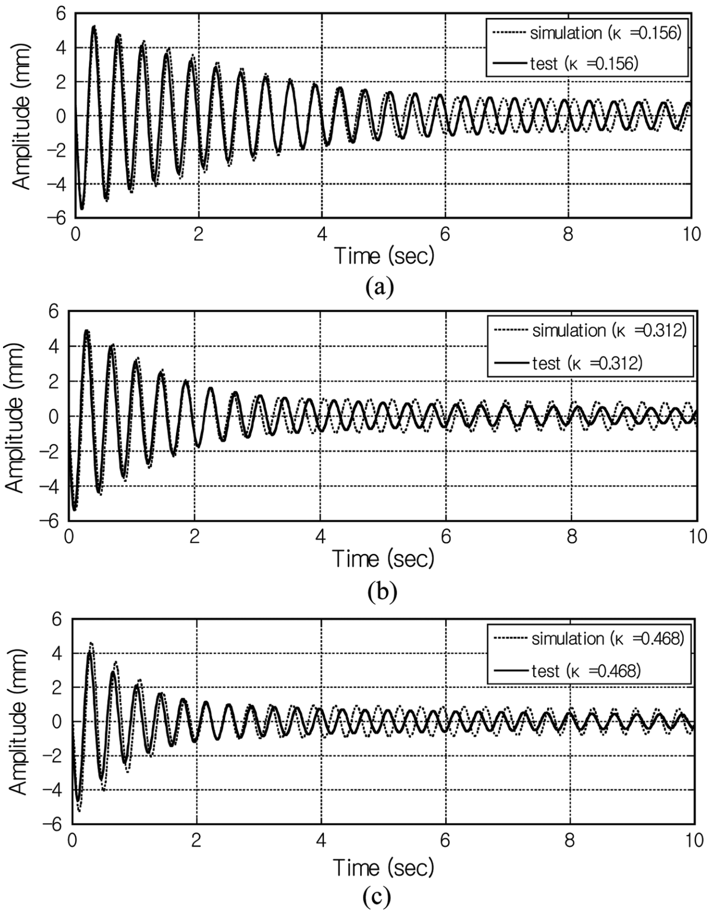

Fig. 13 Free vibration waves of test model and simulation: (a) $\kappa = 0.156$, (b) $\kappa = 0.312$ and (c) $\kappa = 0.468$

Table 4 Evaluation of equivalent damping ratio by logarithmic decrement method

(a) Test model with hysteretic damper ($\kappa = 0.156$)				
Amplitude (mm)	Amplitude ratio (d)	Logarithmic decrement (ln d)	Equivalent damping ratio (h_{eq})	Average of equivalent damping ratio (h_{aver})
3.91	-	-	-	0.0218
3.41	1.15	0.138	0.0219	
2.97	1.15	0.138	0.0219	
2.59	1.15	0.138	0.0219	
2.26	1.15	0.138	0.0219	
2.00	1.14	0.135	0.0215	

(b) Test model with hysteretic damper ($\kappa = 0.312$)				
Amplitude (mm)	Amplitude ratio (d)	Logarithmic decrement (ln d)	Equivalent damping ratio (h_{eq})	Average of equivalent damping ratio (h_{aver})
4.05	-	-	-	0.0389
3.18	1.27	0.241	0.0383	
2.49	1.28	0.246	0.0391	
1.97	1.28	0.246	0.0391	

(c) Test model with hysteretic damper ($\kappa = 0.468$)				
Amplitude (mm)	Amplitude ratio (d)	Logarithmic decrement (ln d)	Equivalent damping ratio (h_{eq})	Average of equivalent damping ratio (h_{aver})
4.34	-	-	-	0.0537
3.09	1.40	0.339	0.0540	
2.21	1.40	0.336	0.0536	
1.67	1.40	0.336	0.0536	

for the response amplitudes. Table 4 presents the equivalent damping ratios of the standard and extended cases. It can be confirmed that the standard case exhibits the targeted damping capacity within a certain amplitude range. Also, the damping capacity of the test models with extended cases is proportional to the stiffness ratio. However, the damping in the response ranges smaller than δ_y depends on the structural damping only. That is, hysteretic dampers are not able to dissipate the energy in the range of small amplitudes. Therefore, it is necessary to reinforce the weak point of the proposed system for another passive control device while maintaining the advantage of the hysteretic damper. In the comparison of the test results with simulations, the test models' natural periods become longer slightly. This phenomenon is remarkable in the responses around 1 mm. It may be caused by the assumption in the simulations that the hysteretic dampers obey normal bilinear hysteretic rules (elastic-perfectly plastic) as well as the geometrical nonlinearity as mentioned in Section 3.2 while the actual hysteretic dampers exhibit hysteretic rules without clear yielding points.

Fig. 14 presents the comparison of the equivalent damping ratio of the standard case with that including the high-hardness rubber dampers (Tani *et al.* 2009). The maximum equivalent damping ratio of the standard case is lower than that of the equivalent linear model as presented in Fig. 6. It results from geometrical nonlinearity as well as the lateral stiffness of the hysteretic damper lower than the design value. However, it can be confirmed that the standard case of the hysteretic damper

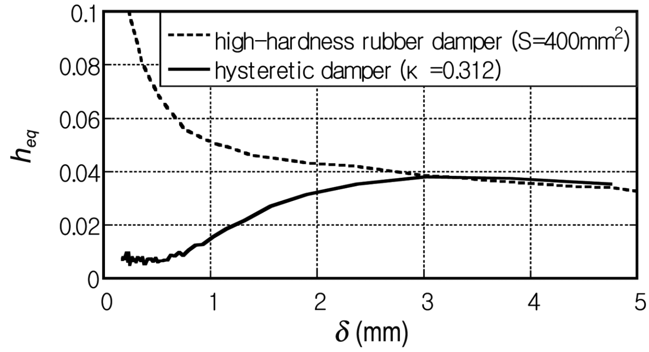

Fig. 14 Comparison of the equivalent damping ratio of the standard case with that of the high-hardness rubber damper with respect to amplitude

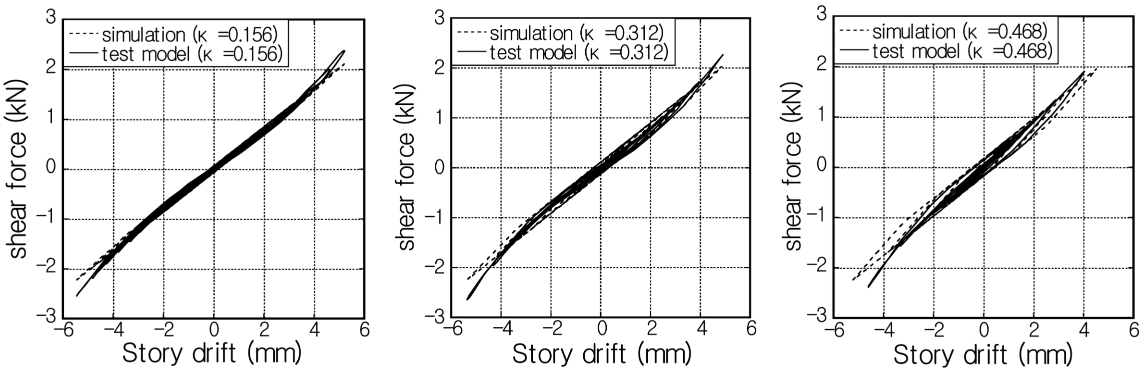

Fig. 15 Comparison of dynamic restoring-force curve of test model with simulation: (a) $\kappa = 0.156$, (b) $\kappa = 0.312$ and (c) $\kappa = 0.468$

exhibits the designed damping capacity $h_{eq} = 0.04$ at the amplitude of 3 mm. The parallel use of the hysteretic dampers and the high-hardness rubber dampers may be one possibility for the construction of an effective damper system. This will be discussed in the future.

Fig. 15 shows the comparison of the dynamic restoring-force curves of the test models with those of the simulations. While the shear forces of the test models correspond well with those of the simulations at the story-drift smaller than 3 mm, the differences in the entire system's shear force become large according to the increase of the stiffness ratio at the story-drift larger than 3 mm. It may be caused by not only the geometrical nonlinearity but also the assumption that the hysteretic dampers obey normal bilinear hysteretic rules (elastic-perfectly plastic).

6. Conclusions

This paper developed a new three-layer pillar-type hysteretic damper system and evaluated its damping capacity. The conclusions may be summarized as follows;

(1) A new three-layer pillar-type hysteretic damper system composed of three layers has been

proposed. The system has a high damping capacity for dynamic loading and also possesses reliable advantages of low cost and ease in installation. The low cost results from the ability of the systematized and mass production of damper units. On the other hand, the characteristic that the overall damper system is divided into a damper unit and brace members leads to ease in installation.
(2) The structural variables used in the design of hysteretic dampers are the stiffness ratio κ, ductility ratio μ_a and the ratio β of the damper's shear force to the maximum resistance. An optimal ductility ratio for maximizing the equivalent damping ratio exists for each stiffness ratio. The designed hysteretic damper exhibits the targeted damping capacity within a certain amplitude range.
(3) The damping capacity of the proposed damper system was verified through the free vibration tests with full-scale models. From the test results, it was confirmed that the damping performance of the proposed system is affected by the geometrical nonlinearity of hysteretic dampers designed for this study. A detailed analytical model considering the geometrical nonlinearity should be used to simulate the damping performance accurately.
(4) Hysteretic dampers are not able to dissipate the energy in the range of amplitudes smaller than the yield deformation amplitude. Therefore, it is necessary to reinforce the weak point by introducing another passive control device in parallel (for example visco-elastic dampers (Tani *et al*. 2008, 2009)) while maintaining the advantage of the hysteretic damper.

Acknowledgements

The authors are grateful for the support of the GCOE program in Kyoto University (Human Security Engineering for Asian Megacities). This project is also partially supported by JSPS (Japan Society for the Promotion of Science).

References

Aiken, I.D., Nims, D.K., Whittaker, A.S. and Kelly, J.M. (1993), "Testing of passive energy dissipation systems", *Earthq. Spectra*, **9**(3), 335-370.
Apostolakis, G. and Dargush, G.F. (2010), "Optimal seismic design of moment-resisting steel frames with hysteretic passive devices", *Earthq. Eng. Struct. D*., **39**(4), 355-376.
Benavent-Climent, A. (2011), "An energy-based method for seismic retrofit of existing frames using hysteretic dampers", *Soil Dyn. Earthq. Eng*., **31**(10), 1385-1396.
Chan, R.W.K. and Albermani, F. (2008), "Experimental study of steel slit damper for passive energy dissipation", *Eng. Struct*., **30**(4), 1058-1066.
Christopoulos, C. and Filiatrault, A. (2006), *Principle of passive supplemental damping and seismic isolation*, IUSS Press, University of Pavia, Italy.
Hanson, R.D. and Soong, T.T. (2001), *Seismic design with supplemental energy dissipation devices*, EERI, Oakland, CA.
Housner, G.W., Bergman, L.A., Caughey, T.K., Chassiakos, A.G., Claus, R.O., Masri, S.F., Skelton, R.E., Soong, T.T., Spencer, B.F. and Yao, J.T.P. (1997), "Special issue, Structural control : past, present, and future", *J. Eng. Mech.-ASCE*, **123**(9), 897-971.
Inoue, K. and Kuwahara, S. (1998), "Optimum strength ratio of hysteretic damper", *Earthq. Eng. Struct. D*., **27**(6), 577-588.
Kim, H.G., Yoshitomi, S., Tsuji, M. and Takewaki, I. (2011), "Development of pillar-type hysteretic damper system composed of three layers and evaluation of its damping capacity", *Proc. of The ASEM11+ Congress*,

Seoul, Korea, 1110-1124.

Kim, J.K. and Seo, Y.L. (2004), “Seismic design of low-rise steel frames with buckling-restrained braces”, *Eng. Struct*., **26**(5), 543-551.

Kozo System (2011), *General-purpose elastic-plastic analysis program for arbitrary-shaped three-dimensional frames (SNAP)*, Tokyo.

Li, H.N. and Li, G. (2007), “Experimental study of structure with “dual function” metallic dampers”, *Eng. Struct*., **29**(8), 1917-1928.

Moreschi, L.M. and Singh, M.P. (2003), “Design of yielding metallic and friction dampers for optimal seismic performance”, *Earthq. Eng. Struct. D*., **32**(8), 1291-1311.

Nakashima, M., Saburi, K. and Tsuji, B. (1996), “Energy input and dissipation behavior of structures with hysteretic dampers”, *Earthq. Eng. Struct. D*., **25**(5), 483-496.

Oh, S.H., Kim, Y.J. and Ryu, H.S. (2008), “Seismic performance of steel structures with slit dampers”, *Eng. Struct*., **31**(9), 1997-2008.

Skinner, R.I., Kelly, J.M. and Heine, A.J. (1975), “Hysteretic dampers for earthquake-resistant structures”, *Earthq. Eng. Struct. D*., **3**(3), 287-296.

Takewaki, I. (2009), *Building control with passive dampers: -Optimal performance-based design for earthquakes-*, John Wiley & Sons Ltd. (Asia).

Tani, T., Yoshitomi, S., Tsuji, M. and Takewaki, I. (2009), “High-performance control of wind-induced vibration of high-rise building via innovative high-hardness rubber damper”, *Struct. Des. Tall Spec*., **18**(7), 705-728.

Tsuji, M., Fujuwara, Y., Murata, S., Kim, H.G., Yoshitomi, S. and Takewaki, I. (2010), “Post-tensioning damper system for micro-vibration reduction in residential houses: Analysis of effective deformation ratio by a simplified model”, *J. Struct. Eng.-AIJ*, **56B** (in Japanese).

Yamaguchi, H. and El-Abd, A.M. (2003), “Effect of earthquake energy input characteristics on hysteretic damper efficiency”, *Earthq. Eng. Struct. D*., **32**(6), 827-843.

CC